J|A|C|S ARTICLES

Published on Web 12/10/2009

Strongly Nonlinear Optical Glass Fibers from Noncentrosymmetric Phase-Change Chalcogenide Materials

In Chung,[†,‡] Joon I. Jang,[§] Christos D. Malliakas,[†] John B. Ketterson,[§] and Mercouri G. Kanatzidis*[,†,‡]

Departments of Chemistry and of Physics and Astronomy, Northwestern University, Evanston, Illinois 60208, and Department of Chemistry, Michigan State University, East Lansing, Michigan 48824

Received October 16, 2009; E-mail: m-kanatzidis@northwestern.edu

Abstract: We report that the one-dimensional polar selenophosphate compounds $APSe_6$ (A = K, Rb), which show crystal−glass phase-change behavior, exhibit strong second harmonic generation (SHG) response in both crystal and glassy forms. The crystalline materials are type-I phase-matchable with SHG coefficients $\chi^{(2)}$ of 151.3 and 149.4 pm V^{-1} for K^+ and Rb^+ salts, respectively, which is the highest among phase-matchable nonlinear optical (NLO) materials with band gaps over 1.0 eV. The glass of $APSe_6$ exhibits comparable SHG intensities to the top infrared NLO material $AgGaSe_2$ without any poling treatments. $APSe_6$ exhibit excellent mid-IR transparency. We demonstrate that starting from noncentrosymmetric phase-change materials such as $APSe_6$ (A = K, Rb), we can obtain optical glass fibers with strong, intrinsic, and temporally stable second-order nonlinear optical (NLO) response. The as-prepared glass fibers exhibit SHG and difference frequency generation (DFG) responses over a wide range of wavelengths. Raman spectroscopy and pair distribution function (PDF) analyses provide further understanding of the local structure in amorphous state of $KPSe_6$ bulk glass and glass fiber. We propose that this approach can be widely applied to prepare permanent NLO glass from materials that undergo a phase-change process.

1. Introduction

Obtaining new coherent light sources involving different frequencies with the potential for tunability is of great importance. Relatively few lasers prove to be practical and commercially viable and they typically generate a single or at best a few optical frequencies. Frequency conversion by a nonlinear optical (NLO) crystal is an effective way of producing coherent light at frequencies where lasers perform poorly or are unavailable. For example, when two incoming frequencies ω_1 and ω_2 are introduced in an NLO medium, they interact to produce four distinct frequencies: $2\omega_1$ and $2\omega_2$ by second harmonic generation (SHG), together with $(\omega_1 \pm \omega_2)$ by sum and difference frequency generation (SFG and DFG).[1] Demand for widely tunable, coherent IR laser sources is emerging. Examples include high-rate (broadband) information transfer for telecommunications and Internet[2] [1.3−1.6 μm via wavelength-division-multiplexing (WDM) all-optical networks[3,4]]; sensing for organic and inorganic molecules[5] (including chemical warfare agents,[6] biohazards,[7] explosives,[8] and pollutants[9]); and medical applications (in the range 2−12 μm).[10]

To be maximally useful, NLO materials should possess phase matchability, high second-order nonlinearity, wide optical transparency, and thermal stability. Many inorganic oxides[11] and polymer NLO materials[12] strongly absorb mid-IR light; in addition, polymers show poor thermal stability and low damage thresholds. A crucial challenge facing many inorganic NLO crystals is the difficulty of fabricating fibers and films, yet some applications require fibers or thin films. Thanks to their IR transparency and high index of refraction (2.2−3.5),[13] chalcogenide glasses are promising contenders for low-loss infrared optical fibers or planar waveguides. Glasses, however, ordinarily lack a second-order optical nonlinearity such as SHG and DFG, because of the presence of inversion symmetry at the macro-

† Department of Chemistry, Northwestern University.
‡ Department of Chemistry, Michigan State University.
§ Department of Physics and Astronomy, Northwestern University.

(1) Bloembergen, N. *Nonlinear optics*, 4th ed.; World Scientific: River Edge, NJ, 1996.
(2) Islam, M. N. *Phys. Today* **1994**, *47*, 34–40.
(3) Chou, M. H.; Brener, I.; Fejer, M. M.; Chaban, E. E.; Christman, S. B. *IEEE Photon. Technol. Lett.* **1999**, *11*, 653–655.
(4) Yoo, S. J. B. *J. Lightwave Technol.* **1996**, *14*, 955–966.
(5) Tittel, F. K.; Richter, D.; Fried, A. *Top. Appl. Phys.* **2003**, *89*, 445–510.
(6) Pushkarsky, M. B.; Webber, M. E.; Macdonald, T.; Patel, C. K. N. *Appl. Phys. Lett.* **2006**, *88*, 044103.
(7) Pestov, D.; Wang, X.; Ariunbold, G. O.; Murawski, R. K.; Sautenkov, V. A.; Dogariu, A.; Sokolov, A. V.; Scully, M. O. *Proc. Natl. Acad. Sci. U.S.A.* **2008**, *105*, 422–427.
(8) Pushkarsky, M. B.; Dunayevskiy, I. G.; Prasanna, M.; Tsekoun, A. G.; Go, R.; Patel, C. K. N. *Proc. Natl. Acad. Sci. U.S.A.* **2006**, *103*, 19630–19634.
(9) Pushkarsky, M.; Tsekoun, A.; Dunayevskiy, I. G.; Go, R.; Patel, C. K. N. *Proc. Natl. Acad. Sci. U.S.A.* **2006**, *103*, 10846–10849.
(10) Jean, B.; Bende, T. *Top. Appl. Phys.* **2003**, *89*, 511–544.
(11) Fossier, S.; Salaun, S.; Mangin, J.; Bidault, O.; Thenot, I.; Zondy, J. J.; Chen, W. D.; Rotermund, F.; Petrov, V.; Petrov, P.; Henningsen, J.; Yelisseyev, A.; Isaenko, L.; Lobanov, S.; Balachninaite, O.; Slekys, G.; Sirutkaitis, V. *J. Opt. Soc. Am. B* **2004**, *21*, 1981–2007.
(12) Park, S. K.; Do, J. Y.; Ju, J. J.; Park, S.; Kim, M. S.; Lee, M. H. *Mater. Lett.* **2005**, *59*, 2872–2875.
(13) Seddon, A. B. *J. Non-Cryst. Solids* **1995**, *184*, 44–50.

10.1021/ja908839s

scopic level. There have been numerous efforts[14] to induce SHG in glasses via poling using thermal,[15] optical,[16] and electron beam irradiation;[17] however, the procedures are complex and/or expensive, and the resulting SHG is too small for practical applications and often nonpermanent. This fact largely restricts the application of glassy silica fiber, the backbone of modern telecommunication systems, to passive devices.

Recently, our pair distribution function (PDF) analysis and Raman spectroscopic studies on the crystal-glass phase-change materials $K_2P_2Se_6$[18] and $K_{1-x}Rb_xSb_5S_8$[19] revealed that their glassy phases still largely preserve the basic building blocks that define the crystal structure; in contrast to a common glass like silica, only the long-range crystallographic order is lost. For the noncentrosymmetric compounds in this class, e.g., $K_2P_2Se_6$[18] and $Cs_5P_5Se_{12}$,[20] we surprisingly observed significant innate SHG response from the as-prepared bulk glassy powders, plausibly by virtue of the noncentrosymmetric fragments partially intact in the glassy form of the phase-change materials. If true, an optical glassy fiber exhibiting intrinsic SHG response can be drawn from the melt of noncentrosymmetric crystal−glass phase-change materials, keeping the advantages of a glass fiber, such as long length, mechanical flexibility, optical transparency, and low optical loss.

Here we report that the one-dimensional selenophosphate compounds $APSe_6$ (A = K, Rb),[21] which crystallize in the noncentrosymmetric polar space group $Pca2_1$, form highly efficient, mechanically flexible nonlinear optical glass fibers without the need of poling.[14] The observed SHG response of the glass fiber can be further significantly enhanced simply by annealing at 260 °C, which converts it to a crystalline fiber.

2. Experimental Section

2.1. Reagents. The reagents mentioned in this work were used as obtained unless noted otherwise: K metal (analytical reagent, Aldrich Chemical Co., Milwaukee, WI); Rb metal (analytical reagent, Aldrich Chemical Co., Milwaukee, WI); red phosphorus powder (99%, Sigma−Aldrich Inc., St. Louis, MO); Se (99.9999%, Noranda Advanced Materials, Quebec, Canada). A_2Se (A = K, Rb) starting materials were prepared by reacting stoichiometric amounts of the elements in liquid ammonia.

2.2. Synthesis. Pure $APSe_6$ (A = K, Rb) was achieved by a stoichiometric mixture of A_2Se:P:Se = 1:2:11 under vacuum in a silica tube at 350 °C for 2 days, followed by cooling at a rate of 5 °C h^{-1} to 250 °C. Energy-dispersive spectroscopic analysis of the crystals showed an average composition of "$KPSe_{6.2}$" and "$Rb_{1.2}PSe_{6.1}$", respectively, for the orange rod-type single crystals. High-purity glassy phases of $APSe_6$ were obtained by quenching the melts of corresponding single crystals to room temperature. A glassy fiber of $APSe_6$ was drawn from the melt near the melting point of each material. Crystal data for $KPSe_6$: orthorhombic $Pca2_1$, $Z = 4$; $a = 11.5052(7)$ Å, $b = 6.7939(6)$ Å, $c = 11.2328(7)$ Å, $V = 878.01(11)$ Å^3 at 100 K. Crystal data for $RbPSe_6$: orthorhombic $Pca2_1$, $Z = 4$; $a = 11.776(2)$ Å, $b = 6.858(1)$ Å, $c = 11.776(2)$ Å, $V = 925.5(2)$ Å^3 at 293 K. $KPSe_6$ mp ∼320 °C; $RbPSe_6$ mp ∼315 °C (Supporting Information, Figure S1).

2.3. Physical Measurements. 2.3.1. X-ray Powder Diffraction. Analyses for powder samples were performed on a calibrated CPS 120 INEL X-ray powder diffractometer (Cu Kα radiation) operating at 40 kV/20 mA and equipped with a position-sensitive detector with flat sample geometry. Fibers were examined with a STOE II single-crystal diffractometer (Ag Kα radiation) at 100 K.

2.3.2. Electron Microscopy. Semiquantitative analyses of the compounds were performed with a JEOL JSM-35C scanning electron microscope (SEM) equipped with a Tracor Northern energy-dispersive spectroscopy (EDS) detector. SEM images were taken with a Hitachi S-3400N-II variable-pressure SEM.

2.3.3. Solid-State UV−Vis Spectroscopy. Optical diffuse reflectance measurements were performed at room temperature on a Shimadzu UV-3101 PC double-beam, double-monochromator spectrophotometer operating in the 200−2500 nm region. The instrument is equipped with an integrating sphere and controlled by a personal computer. $BaSO_4$ was used as a 100% reflectance standard. The sample was prepared by grinding the crystals to a powder and spreading the powder on a compacted surface of the powdered standard material, preloaded into a sample holder. The reflectance versus wavelength data generated were used to estimate the band gap of the material by converting reflectance to absorption data[22−24] according to Kubelka−Munk equations: $\alpha/S = (1 - R)^2/2R$, where R is the reflectance and α and S are the absorption and scattering coefficients, respectively.

2.3.4. Raman Spectroscopy. Raman spectra were recorded on a Holoprobe Raman spectrograph equipped with a charge-coupled device (CCD) camera detector, with 633 nm radiation from a HeNe laser for excitation and a resolution of 4 cm^{-1}. Laser power at the sample was estimated to be about 5 mW, and the focused laser beam diameter was ca. 10 μm. A total of 128 scans was sufficient to obtain good quality spectra.

2.3.5. Infrared Spectroscopy. Fourier transform infrared (FT-IR) spectra were recorded as solids in a CsI or KBr matrix. The samples were ground with dry CsI or KBr into a fine powder and pressed into translucent pellets. The spectra were recorded in the far-IR region (600−100 cm^{-1}, 2 cm^{-1} resolution) and mid-IR region (500−4000 cm^{-1}, 2 cm^{-1} resolution) with the use of a Nicolet 6700 FT-IR spectrometer equipped with a TGS/PE detector and silicon beam splitter.

2.3.6. Differential Thermal Analysis. Experiments were performed on a Shimadzu DTA-50 thermal analyzer. A sample (∼30 mg) of ground crystalline material was sealed in a silica ampule under vacuum. A similar ampule of equal mass filled with Al_2O_3 was sealed and placed on the reference side of the detector. The sample was heated to 500 °C at 10 °C min^{-1}, and after 1 min it was cooled at a rate of −10 °C min^{-1} to 50 °C. The residues of the differential thermal analysis (DTA) experiments were examined by X-ray powder diffraction. Reproducibility of the results was confirmed by running multiple heating/cooling cycles. The melting and crystallization points were measured at a minimum endothermic peak and a maximum exothermic peak.

2.3.7. Nonlinear Optical Property Measurements. We used the frequency-tripled output (355 nm) of a passive−active mode-

(14) Margulis, W.; Garcia, F. C.; Hering, E. N.; Valente, L. C. G.; Lesche, B.; Laurell, F.; Carvalho, I. C. S. *MRS Bull.* **1998**, *23*, 31–35.
(15) Myers, R. A.; Mukherjee, N.; Brueck, S. R. J. *Opt. Lett.* **1991**, *16*, 1732–1734.
(16) Corbari, C.; Kazansky, P. G.; Slattery, S. A.; Nikogosyan, D. N. *Appl. Phys. Lett.* **2005**, *86*, 071106.
(17) Kazansky, P. G.; Dong, L.; Russell, P. S. *Opt. Lett.* **1994**, *19*, 701–703.
(18) Chung, I.; Malliakas, C. D.; Jang, J. I.; Canlas, C. G.; Weliky, D. P.; Kanatzidis, M. G. *J. Am. Chem. Soc.* **2007**, *129*, 14996–15006.
(19) Wachter, J. B.; Chrissafis, K.; Petkov, V.; Malliakas, C. D.; Bilc, D.; Kyratsi, T.; Paraskevopoulos, K. M.; Mahanti, S. D.; Torbrugge, T.; Eckert, H.; Kanatzidis, M. G. *J. Solid State Chem.* **2007**, *180*, 420–431.
(20) Chung, I.; Jang, J. I.; Gave, M. A.; Weliky, D. P.; Kanatzidis, M. G. *Chem. Commun.* **2007**, 4998–5000.
(21) Chung, I.; Do, J.; Canlas, C. G.; Weliky, D. P.; Kanatzidis, M. G. *Inorg. Chem.* **2004**, *43*, 2762–2764.
(22) Tandon, S. P.; Gupta, J. P. *Phys. Status Solidi* **1970**, *38*, 363–367.
(23) (a) Chung, D. Y.; Choi, K. S.; Iordanidis, L.; Schindler, J. L.; Brazis, P. W.; Kannewurf, C. R.; Chen, B. X.; Hu, S. Q.; Uher, C.; Kanatzidis, M. G. *Chem. Mater.* **1997**, *9*, 3060–3071. (b) Chondroudis, K.; McCarthy, T. J.; Kanatzidis, M. G. *Inorg. Chem.* **1996**, *35*, 840–844. (c) Kanatzidis, M. G.; Huang, S. P. *Inorg. Chem.* **1989**, *28*, 4667–4669.
(24) (a) Stephan, H. O.; Kanatzidis, M. G. *Inorg. Chem.* **1997**, *36*, 6050–6057. (b) McCarthy, T. J.; Kanatzidis, M. G. *Inorg. Chem.* **1995**, *34*, 1257–1267.

locked Nd:YAG laser with a pulse width of about 30 ps and a repetition rate of 10 Hz to pump an optical parametric amplifier (OPA). The OPA generates vertically polarized pulses in the range 400−3156 nm. In order to study the wave-guided SHG response from our glass fiber, we used the idler beam (λ_{idler} = 1240−1610 nm) from the same OPA setting as above. The incident laser pulse of 0.2 mJ was focused onto the proximal surface of a fiber with a spot 300 μm in diameter by use of a 3 cm focal-length parabolic lens. The diameter of this fiber was about 122 ± 2 μm and its length is 10 mm. The corresponding instantaneous peak power is about 6.7 MW. Considering the low pulse repetition rate of 10 Hz, however, the time-average input fluence is only 2.8 W cm^{-2}, well below the damage threshold for chalcogenide compounds.[25] Although the corresponding peak fluence is about 9 GW cm^{-2}, which can induce third harmonic response of the test material, no third-harmonic generation was detected, even with an extended collection time. By selectively focusing the imaging lens on the opposite distal end of the fiber, the SHG signals were collected in a wave-guided mode and dispersed with a Spex Spec-One 500 M spectrometer coupled to a nitrogen-cooled CCD camera. Since our monitoring range in the wavelength is rather wide, we did not use any filter but made sure that other optical components did not generate additional SHG signals. The SHG response from powder samples was measured via reflection geometry under similar conditions.

2.3.8. Atomic Pair Distribution Function Analysis. Crystalline and glassy fine powder (<40 μm) and glassy fibers ($d \sim$ 50 and 200 μm) of $KPSe_6$ were measured. Diffraction data were collected at room temperature by the rapid acquisition pair distribution function technique.[26] Data were collected with an MAR345 image plate detector and ~60 keV energy X-rays (λ = 0.2128 Å) at the 11-ID-B beamline at the Advanced Photon Source. Measurements were repeated 4−5 times per sample to improve counting statistics. The data were combined and integrated by use of the program FIT2D.[27] Various corrections were made to the data, such as subtraction of background, Compton and fluorescence scattering, geometric corrections, absorption, and so on, as described in ref 28. Corrections were made with the program PDFgetX2.[29] Structural model was fit to the data by use of the program PDFFIT.[30]

3. Results and Discussion

3.1. Crystal Structure and Optical Transmittance. The structure of these two compounds has infinite chains of $_\infty^1[PSe_6^-]$, consisting of the $[PSe_4]$ tetrahedral units condensed with Se_2 linkages (Figure 1A). The easily polarizable P and Se atoms linked by covalent bonding produce a large optical nonlinearity. The compounds exhibit reversible crystal−glass phase-change behavior with optical contrast between the phases: crystalline $KPSe_6$, 2.16 eV, and glass, 1.82 eV; crystalline $RbPSe_6$, 2.18 eV, and glass, 1.91 eV. They exhibit wide optical transparency, ranging from long-wave infrared (LWIR) to near-IR/visible light: 19.0 μm−574 nm, crystalline $KPSe_6$, and 19.5 μm−681 nm, glassy $KPSe_6$; 20.2 μm−568 nm, crystalline $RbPSe_6$, and 18.9 μm−649 nm, glassy $RbPSe_6$ (Figure 1B). At energies above those where the complex P−Se absorptions cut off in the far-IR region, uninterrupted light transmission continues through the mid-IR region. The optical transparency extends to the fundamental absorption edge of the compounds in the visible region. By comparison, the benchmark NLO material for IR applications $AgGaSe_2$ shows LWIR transmission up to 17 μm.[31]

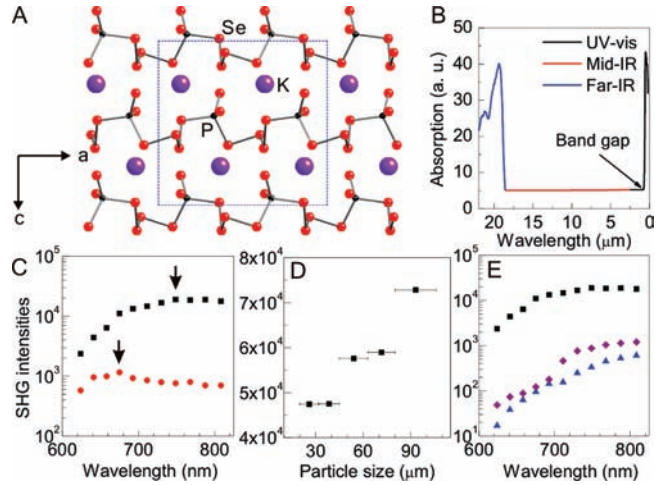

Figure 1. Crystal structure, optical transparency, and SHG measurements of $KPSe_6$. (A) Unit cell viewed down the *b*-axis. (B) Far-IR/mid-IR/visible absorption spectra of $KPSe_6$ bulk glass showing wide transparency range. (C) Relative SHG intensities of $KPSe_6$ crystal (■) and $AgGaS_2$ (●). Arrow marks indicate the plateau region of SHG intensities, where multiphoton absorption is minimal. (D) Particle size to SHG intensity diagram of crystalline $RbPSe_6$ indicating type I phase-matching. (E) Relative SHG intensities of $KPSe_6$ crystal (■), $KPSe_6$ glass (▲), and $AgGaSe_2$ (◆).

3.2. Second Harmonic Generation Response of Crystalline and Glassy $APSe_6$ (A = K, Rb). As a part of this work, we examined SHG responses of crystalline and bulk glassy powders of $APSe_6$ (A = K, Rb) compounds, with various fundamental wavelengths λ ranging from 1240 to 1610 nm, using a modified Kurtz powder method.[32] Input light pulses were generated by an optical parametric amplifier driven by a Nd:YAG pulsed laser at 355 nm with a repetition rate of 10 Hz. Crystalline $APSe_6$ (A = K, Rb) powder generated very strong second harmonic signals over a wide range in the visible/near-infrared region (Figure 1C); the responses increase with particle size, indicating type I phase-matching in our observation range (Figure 1D). We used $AgGaS_2$ powder prepared in a similar fashion as a reference since it is also phase-matchable in the wavelength range of interest, with the well-established value of $\chi_{ref}^{(2)}$ = 36 pm V^{-1}.[25] In order to estimate the absolute value of $\chi^{(2)}$, the SHG intensities of crystalline $KPSe_6$ were directly compared with those of $AgGaS_2$ for the same particle size (137.5 ± 12.5 μm) (Figure 1C). Note the SHG intensities must be compared in the plateau region, indicated by arrows in Figure 1C, where multiphoton absorption is minimal. The absolute $\chi^{(2)}$ was calculated as $\chi^{(2)} = \chi_{ref}^{(2)} (I^{2\omega}/I^{2\omega}{}_{ref})^{1/2}$ = 146.4 ± 5.2 pm V^{-1} for the phase-matchable case,[32] where $I^{2\omega}$ and $I^{2\omega}{}_{ref}$ are the measured SHG intensities from our sample and the reference, respectively. These values for $APSe_6$ compounds are the highest among phase-matchable NLO materials with band gaps over 1.0 eV. Our experimental $\chi^{(2)}$ is reasonably consistent with the theoretical estimate based on highly precise full-potential

(25) Bhar, G. C. *Jpn. J. Appl. Phys., Part 1* **1993**, *32*, 653–659.
(26) (a) Chupas, P. J.; Qiu, X. Y.; Hanson, J. C.; Lee, P. L.; Grey, C. P.; Billinge, S. J. L. *J. Appl. Crystallogr.* **2003**, *36*, 1342–1347. (b) Billinge, S. J. L.; Kanatzidis, M. G. *Chem. Commun.* **2004**, 749–760.
(27) Hammersley, A. P.; Svensson, S. O.; Hanfland, M.; Fitch, A. N.; Hausermann, D. *High Pressure Res.* **1996**, *14*, 235–248.
(28) Egami, T.; Billinge, S. J. L.; *Underneath the Bragg peaks: structural analysis of complex materials*; Pergamon: Oxford, U.K., and Boston, 2003.
(29) Qiu, X. Y.; Bozin, E. S.; Juhas, P.; Proffen, T.; Billinge, S. J. L. *J. Appl. Crystallogr.* **2004**, *37*, 110–116.
(30) Proffen, T.; Billinge, S. J. L. *J. Appl. Crystallogr.* **1999**, *32*, 572–575.
(31) Nikogosyan, D. N. *Nonlinear optical crystals: a complete survey*, 1st ed.; Springer: New York, 2005.
(32) Kurtz, S. K.; Perry, T. T. *J. Appl. Phys.* **1968**, *39*, 3798–3813.

linearized augmented plane-wave (FLAPW)[33] electronic structure calculations at the density functional theory level, which yield $\chi^{(2)} = 151.3$ and 149.4 pm V^{-1} for K^+ and Rb^+ salts.[34] The theoretical study of the compounds concluded that it is a one-dimensional structural anisotropy with a strong covalent character that yields very large second-harmonic coefficients of $APSe_6$ compounds. Accordingly, exploratory synthesis of low-dimensional materials is requested for new NLO crystals. Note that many top-tier, mainstream IR NLO materials are high-symmetric chalcopyrite compounds, for example, $ZnGeP_2$ and $AgGaQ_2$ (Q = S, Se). Despite an exceptional SHG coefficient, $CdZnAs_2$ ($\chi^{(2)} \sim 434$ pm V^{-1}) is only transparent beyond 4 μm, while optically isotropic GaAs ($\chi^{(2)} \sim 240$ pm V^{-1}) is non-phase-matchable.[35]

Unlike crystalline $APSe_6$ (A = K, Rb), the particle-size dependence indicates that glassy $KPSe_6$ is not phase-matchable, as expected for a nominally isotropic material. Therefore, we directly compared glassy $KPSe_6$ with crystalline $AgGaSe_2$, which is also not phase-matchable in our spectral observation range. Considering the large $\chi^{(2)} = 66$ pm V^{-1} for crystalline $AgGaSe_2$,[25] it is remarkable that the glass of $KPSe_6$ exhibits comparable SHG intensities. However, estimation of $\chi^{(2)}$ by the same technique for non-phase-matchable materials requires the coherence length l_c, which is not generally accessible for chalcogenide compounds with typical l_c much smaller than the minimum powder size of 20 μm that we can prepare. The l_c for $AgGaSe_2$ at $\lambda = 1.6$ μm is $\sim$3 μm.[31]

3.3. Fabrication of Optical Glassy Fiber. On the basis of the strong SHG response and wide optical transparency in the IR region of both the crystalline and glassy phases of $APSe_6$ (A = K, Rb), we fabricated optical glass fibers. The fiber drawing process was based upon the reversible thermal behavior of crystal−glass phase-change materials: upon heating, the glassy phase crystallizes, followed by subsequent melting; but upon cooling, only vitrification occurs, rather than recrystallization (Supporting Information, Figure S1). We drew $APSe_6$ glassy fiber from a viscous melt at $\sim$230−280 °C; on cooling from the liquid phase, and between vitrification and the melting point, a continuous viscosity−temperature dependence exists that makes high-speed drawing possible.[36] We note the processing temperature of the chalcogenide fibers is considerably lower than that of oxides. For example, silica fiber requires approximately 2000 K for softening.[37] Fibers with thickness ranging from a few to a hundred micrometers, having remarkable flexibility, could be prepared "by hand" with lengths approaching a meter (Figure 2A). As seen in the scanning electron microscope (SEM) image of Figure 2B, a representative $d = 50.0$ μm fiber displays a high degree of thickness uniformity and surface smoothness; the cross-section of a fiber was continuous with no bubbles or cracks. $KPSe_6$ glassy fiber could recover its crystallinity by annealing it at 260 °C for 3 min. An X-ray diffraction study of pristine fiber on a single-crystal diffractometer showed only diffuse scattering, confirming its dominant amorphous nature, whereas that of annealed fiber showed strong Bragg scattering revealing crystallinity (Figure 3A,B).

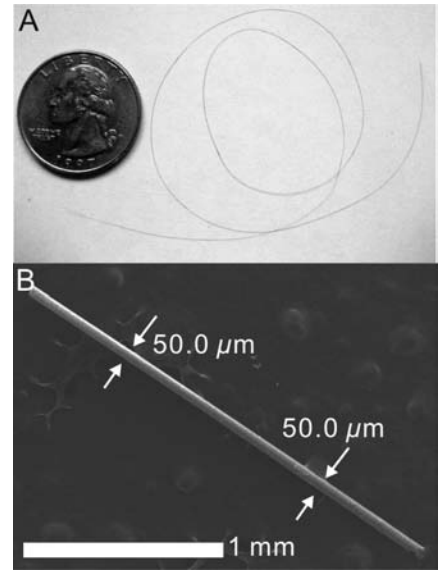

Figure 2. (A) Representative photograph of an optical fiber showing remarkable flexibility. (B) Representative SEM image of a fiber showing thickness uniformity at 50.0 μm and surface smoothness.

3.4. Local Structure. The Raman spectrum of crystalline $KPSe_6$ at room temperature shows major shifts at 220 (s), 231 (m), and 246 (m) cm^{-1} (Figure 3C). The shift at 220 cm^{-1} is unambiguously assigned to the PSe_4 stretching mode by comparing with the A_g stretching mode of the T_d symmetry of $[PSe_4]^{3-}$ ligand. The shifts at 231 and 246 cm^{-1} can be assigned to antisymmetric and symmetric Se−Se stretching modes of the diselenide group, respectively.[18] The Raman spectra of $KPSe_6$ bulk glassy powder and glassy fiber are identical, showing the broader and weaker peaks at 220 (br m) and 259 (br m) cm^{-1}, whereas the overall peak pattern is similar to that of the crystal. This suggests that the $[PSe_4]$ building blocks and Se−Se bonds are still intact and local structural motifs are largely preserved in the bulk glass and glassy fiber, but the long-range crystallographic order is lost. The PDF of bulk glass and glassy fiber shows well-defined correlations up to $\sim$12 Å with the maxima at 2.3 Å (P−Se and Se−Se bonds) and 3.7 Å (K···Se and second-neighbor Se···Se distances) being very close to those of the crystalline phase (Figure 4). This is also in agreement with the Raman spectroscopic data. Above $\sim$12 Å, the PDFs decay rapidly to zero, indicating the loss of long-range order. Those observations support the facile restoration of the crystal structure from the amorphous state at the reversible crystal−glass phase transition. The Raman spectrum of annealed fibers is same as that of bulk crystals, confirming the recovery of crystalline structure in the fiber form (see Figure 3A,B).

3.5. Second-Order Nonlinear Optical Properties of $KPSe_6$ Glassy Fiber. Since the bulk glass powder showed significant SHG response, we examined the corresponding generation and guiding of NLO light in glassy fibers. Being careful to precisely align the fiber with the laser path, we focused the tunable incident beam ($\lambda = 1240$−1610 nm) onto the proximal end of the fiber ($d = 122$ μm, $l = 10.0$ mm); wave-guided outgoing light was collected from the distal end. As-prepared $APSe_6$ glass fibers act as frequency converters in wave-guided mode. The fibers produced continuously tunable SHG signal over a wide range of wavelengths (640−805 nm) (Figure 5A). The decreased

(33) Wimmer, E.; Krakauer, H.; Weinert, M.; Freeman, A. J. *Phys. Rev. B* **1981**, *24*, 864–875.
(34) Song, J.-H.; Freeman, A. J.; Bera, T. K.; Chung, I.; Kanatzidis, M. G. *Phys. Rev. B* **2009**, *79*, 245203.
(35) Fiore, A.; Berger, V.; Rosencher, E.; Bravetti, P.; Nagle, J. *Nature* **1998**, *391*, 463–466.
(36) Abouraddy, A. F.; Bayindir, M.; Benoit, G.; Hart, S. D.; Kuriki, K.; Orf, N.; Shapira, O.; Sorin, F.; Temelkuran, B.; Fink, Y. *Nat. Mater.* **2007**, *6*, 336–347.
(37) Tong, L. M.; Gattass, R. R.; Ashcom, J. B.; He, S. L.; Lou, J. Y.; Shen, M. Y.; Maxwell, I.; Mazur, E. *Nature* **2003**, *426*, 816–819.

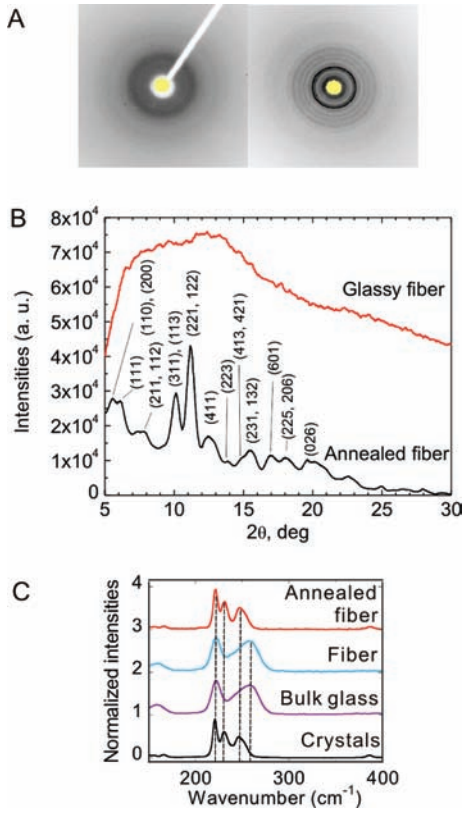

Figure 3. (A) X-ray diffraction ring patterns of pristine glassy (left) and annealed fiber (right), confirming their amorphous and crystalline nature, respectively. (B) X-ray diffraction patterns of the pristine glassy (upper trace) and annealed fibers (lower trace). Diffraction profiles were regenerated from the ring patterns presented in panel A, collected by STOE II single-crystal diffractometer (Ag Kα). Note that the Bragg peaks from the annealed fiber are successfully indexed, indicative of the restoration of crystal structure on the fiber. (*hkl*) index on the major peak is presented. (C) Raman spectra of $KPSe_6$ crystal, bulk glass, pristine glassy fiber, and annealed fiber.

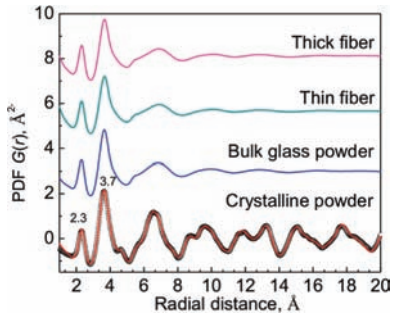

Figure 4. Pair distribution function (PDF) analysis for glassy fiber, bulk glass, and crystalline powders. Fibers with different thickness at $d \sim 50$ μm and $d \sim 200$ μm were examined for comparison. Theoretical fit based upon single-crystal structure refinement is plotted as black circles.

SHG signal below 700 nm is due to the two-photon-induced absorption beyond the band gap. The negligible $\chi^{(3)}$ response from $APSe_6$ was independently confirmed through the absence of a Z-scan response. The observation of intrinsic SHG response from $KPSe_6$ glassy fibers is consistent with that found in the corresponding bulk glass powder. Note the SHG signal is generated continuously along the path, but the full path represents a macroscopic distance of 10.0 mm. In the absence of any innate NLO fiber available at this time, our first observation of macroscopic generation and propagation of SHG light along glass fibers, in addition to being novel, foreshadows

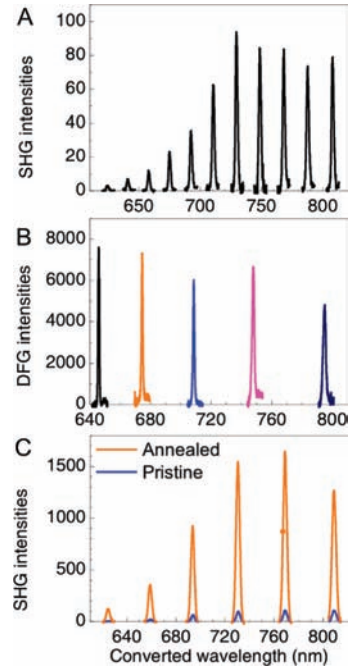

Figure 5. NLO properties of $KPSe_6$ optical glassy fiber over a wide range of vis/near-IR region. (A) Wave-guided SHG response transmitted through 10.0 mm long $KPSe_6$ glassy fiber. (B) DFG response as a function of λ_{idler}, demonstrating wave-mixing capability over a wide range of wavelengths (λ_{idler} = 1575.0, 1497.4, 1420.5, 1350.1, and 1282.1 nm; λ_{signal} = 646.4, 675.1, 709.8, 748.8, and 795.6 nm, from left to right). (C) Relative SHG intensities measured from 620 to 805 nm for the pristine glassy and annealed fibers, representing remarkable enhancement of the SHG response after heat treatment at 260 °C for 3 min.

practical applications. Regarding the materials themselves, further understanding of the temperature dependence, surface tension and viscosity of the melt, the use of high-purity starting materials, and a more sophisticated mechanical drawing process all promise that much higher quality of the fibers is possible.

We also performed DFG experiments, a process that is especially important for generating mid-IR light and facilitates multichannel conversion. Here we used both the signal and idler output beams of the optical parametric amplifier (OPA). The energy conservation among these two beams requires $1/\lambda_{signal} + 1/\lambda_{idler} = 1/355$ nm, and by the definition of DFG, $1/\lambda_{signal} - 1/\lambda_{idler} = 1/\lambda_{DFG}$. Thus, for a given λ_{idler}, the expected wavelength for DFG was

$$\lambda_{DFG} = \left(\frac{\lambda_{idler}}{\lambda_{idler} - 710\ \text{nm}}\right)355\ \text{nm}$$

By introducing different combinations of idler and signal beams, the $KPSe_6$ glass fiber successfully generated continuously tunable near-IR light by DFG (Figure 5B). Deviation among DFG intensities arose from the signal beam, which was beyond the band gap. Although our detection limit (<1 μm) prohibited observing DFG at mid-IR, $APSe_6$ (A = K, Rb) should also produce tunable coherent light throughout the mid-IR region because the compounds are optically transparent there, a region where few NLO materials are available.[35] We could not study SFG because our experimental setup produces constant λ_{SFG} at 355 nm, light that is strongly absorbed through the over-the-gap excitation of the material.

Phase-change materials are of great interest for emerging technologies, including rewritable optical media and the devel-

opment of nonvolatile phase-change memory.[38] Conversion between the crystalline and glassy states can be driven by applying voltage or heat or by irradiating with an appropriate laser. The stoichiometric compounds $APSe_6$ (A = K, Rb) can switch between the crystalline and glassy states without complications arising from compositional changes. We exploited this property to switch the NLO properties of $APSe_6$ fibers. We annealed $KPSe_6$ fibers at 260 °C for 3 min and measured the wave-guided SHG response. Remarkably, the annealed fiber exhibited over 10 times larger SHG intensities compared to the pristine glassy fiber in a wide range of wavelengths (Figure 5C). Note, however, that this enhancement is still a factor of 10 below the SHG intensity changes between the glassy and crystalline powders shown in Figure 1E. This deficit most likely arises from partial cancellation from random distributions of macroscopic grain boundaries with various polarization directions. Other possible mechanisms could be random phase matching (RPM), since SHG intensity arising from RPM increases linearly with the NLO medium size.[39]

4. Concluding Remarks

We presented a new concept on how to create stable NLO glass fibers. Namely, noncentrosymmetric phase-change materials can be used to quench an NLO-active glass phase from which fibers with stable SHG properties can be drawn. We demonstrated this with $APSe_6$ fibers, which possess intrinsic, switchable second-order NLO properties with the strongest response known for glasses. The concept suggested here is an example of combining apparently unrelated properties (NLO + phase-change behavior) to create new functional materials. This finding could open up new possibilities of creating active, all-optical, broadband networks that independently modulate frequency, with no additional NLO or electronic devices.

Acknowledgment. We acknowledge the National Science Foundation for financial support (Grants DMR-0801855, FRG-0703382, and 0306731 U.S./Ireland cooperation) and the Northwestern University Materials Research Center (under NSF Grant DMR-0520513).

Supporting Information Available: One figure showing (A) DTA diagram and (B) X-ray powder diffraction patterns of glass and restored crystal of $RbPSe_6$. This material is available free of charge via the Internet at http://pubs.acs.org.

JA908839S

(38) Wuttig, M.; Yamada, N. *Nat. Mater.* **2007**, *6*, 824–832.

(39) Baudrier-Raybaut, M.; Haidar, R.; Kupecek, P.; Lemasson, P.; Rosencher, E. *Nature* **2004**, *432*, 374–376.